Supplementary Figures: 9

Supplementray Figure S1

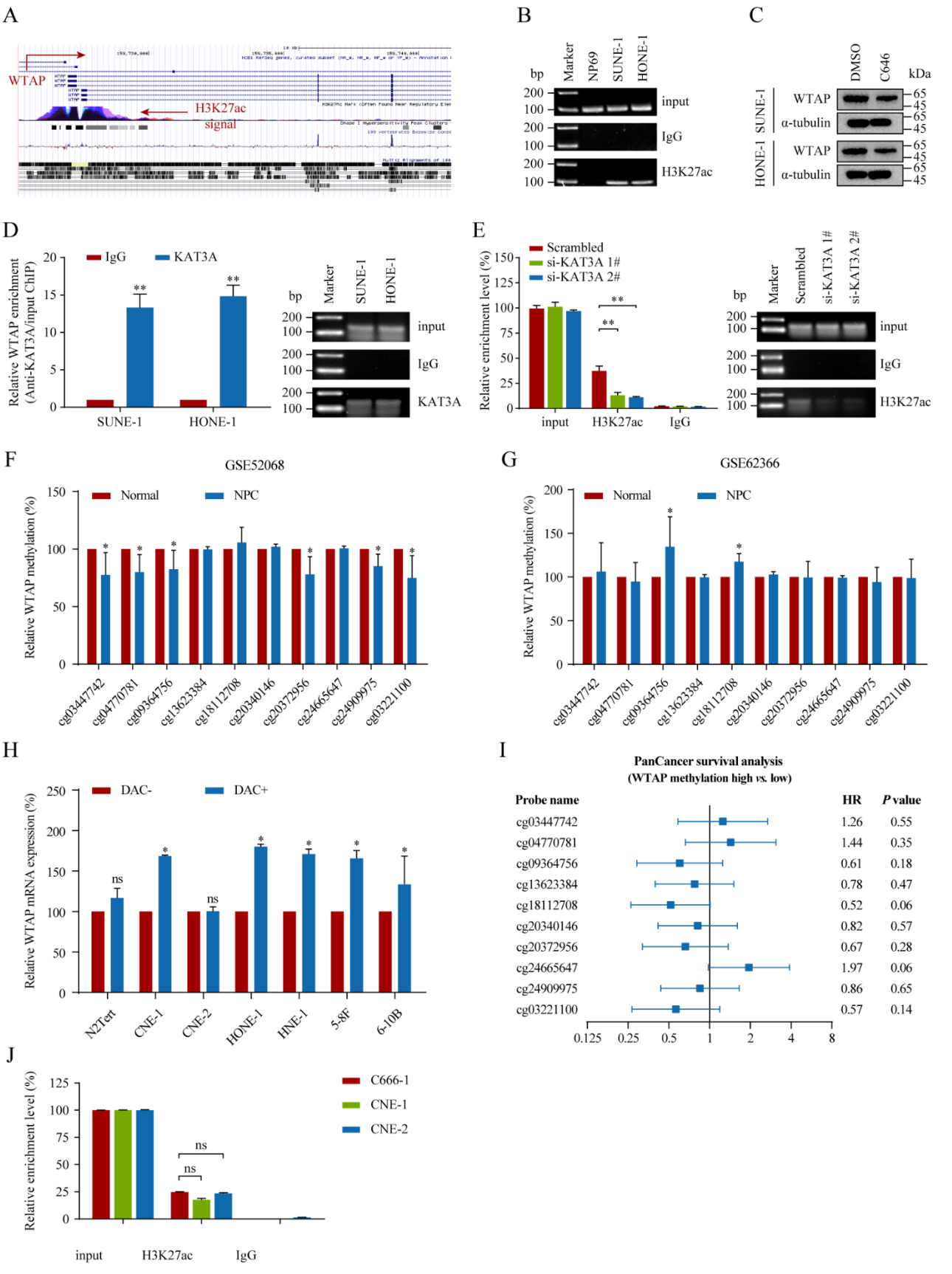

Supplemental Figure S1. KAT3A-mediated H3K27ac activates WTAP transcription in NPC.

A. The UCSC Genome Browser (http://genome.ucsc.edu/) showed that the promoter region of WTAP was highly enriched with of H3K27ac. **B.** The result of ChIP-qPCR in Figure 1I was visualized by DNA electrophoresis through 1% agarose. **C.** WTAP expression was measured by western blotting in SUNE-1 and HONE-1 cells treated with C646 (10μM) or DMSO for 48 h. **D.** ChIP-PCR assay using anti-KAT3A antibody assessed its enrichment at the WTAP promoter. **E.** The enrichment of H3K27ac at the WTAP promoter was evaluated by a ChIP-PCR assay in HONE-1 cells with KAT3A silencing. **F–G.** The relative DNA methylation level of WTAP was assessed based on our previous microarray data (GSE52068, **F**) and the Hong Kong microarray data (GSE62336, **G**). **H.** Quantitative RT-PCR analysis of WTAP expression in one immortalized nasopharyngeal epithelial cell line (N2Tert) and six NPC cell lines (CNE-1, CNE-2, HONE-1, HNE-1, 5-8F and 6-10B). Cells were treated with DAC (10 μM)) for 72h and harvested for analysis (DAC+). PBS buffer treatment was used as a mock control (DAC-). **I.** Hazard ratio (HR) plot of the WTAP methylation level (high vs. low) by prognostic factors for overall survival. Data were obtained from the online tool MethSurv based on the DNA methylation and clinical information using TCGA (The Cancer Genome Atlas) dataset. **J.** H3K27 acetylation in WTAP promoters was measured by ChIP-qPCR. NPC cells with EBV positive (C666-1) and EBV-negative (CNE-1 and CNE-2) were used. Data are presented as the mean ± SD. **P* < 0.05, ***P* < 0.01. The experiments were repeated at least three times independently.

Supplementray Figure S2

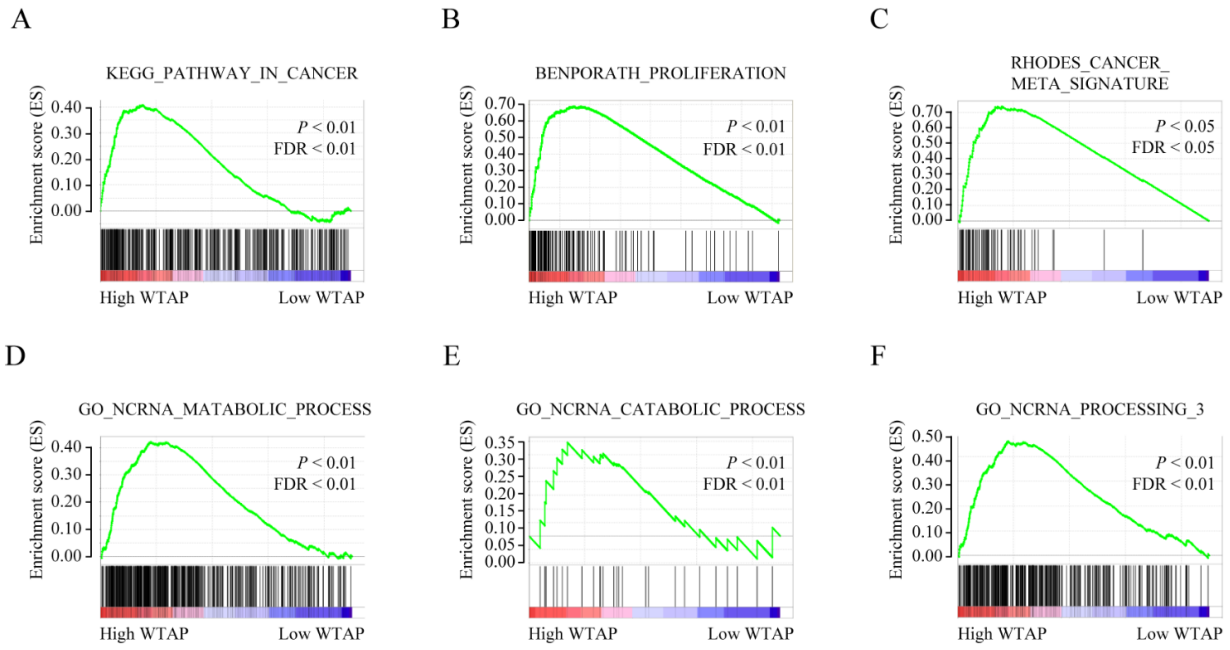

Supplemental Figure S2. WTAP may serve as an oncogenic role in NPC.

A–G. GSEA analysis reveals the molecular and biological signatures of WTAP in NPC based on the GEO database (GSE12452), indicating that “Pathway in cancer” (**A**), “Cancer proliferation” (**B**), “Cancer metastasis” (**C**), and “Non-coding RNA processing” (**D–F**) signatures between WTAP high expression samples versus WTAP low expression samples.

Supplementary Figure S3

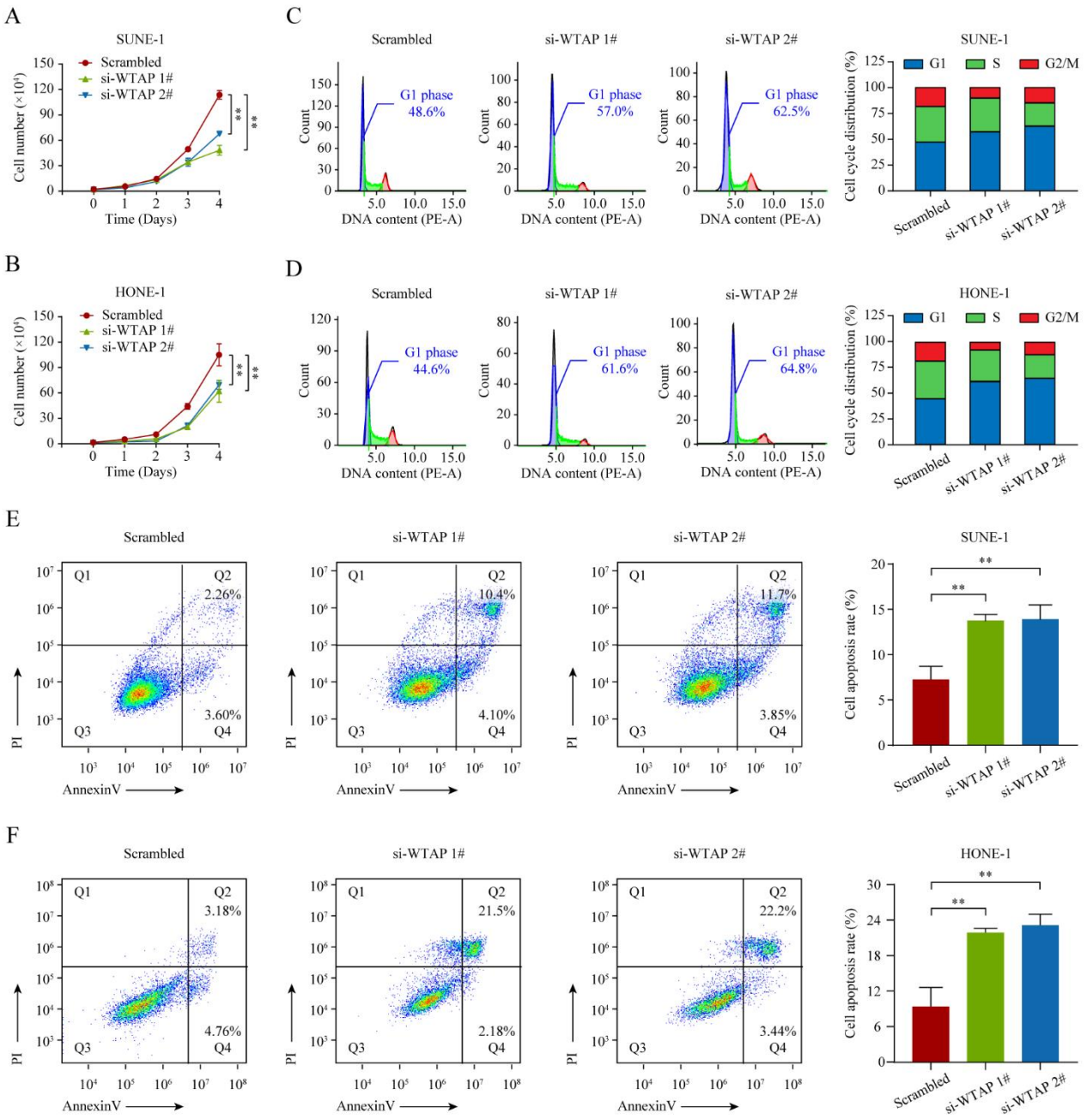

Supplemental Figure S3. Silencing WTAP impairs the proliferation ability of NPC cell *in vitro*. **A–B.** Cell proliferation was evaluated by the cell counting method. 48h after transfection, the NPC cells were seeded in 12-well culture plates at a density of 2×10^4 per well and left overnight at 37℃ in a humidified incubator with 5% CO_2. Then the cells were trypsinized and counted at time zero (Day 0), 1, 2, 3, and 4 days. The SUNE-1 (**A**) and HONE-1 (**B**) cells were counted three times by three independent experimenters. **C–F.** FACS analysis in SUNE-1 and HONE-1 cells transfected with si-WTAP or scramble control. Cells were collected, stained with propidium iodide (PI) for cell cycle

analysis (**C–D**) or with Annexin-V-FITC and PI for apoptosis analysis (**E–F**). Graphical and statistical analyses for the cell cycle distribution (G1, S, G2/M phases) of SUNE-1 (**C**) and HONE-1 (**D**) cells. Representative images and statistical analysis of cellular apoptosis portion of SUNE-1 (**E**) and HONE-1 cells (**F**). Data are presented as the mean ± SD. **P* < 0.05, ***P* < 0.01. The experiments were repeated at least three times independently.

Supplementray Figure S4

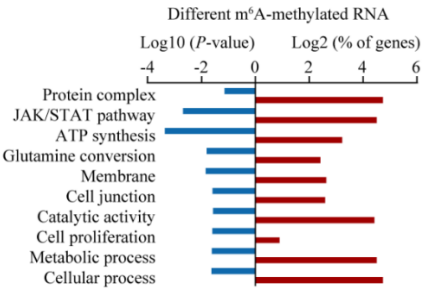

Supplemental Figure S4. PANTHER analysis of enriched functional gene categories of differential m^{6}A methylation genes after WTAP silencing.

.

Supplementary Figure S5

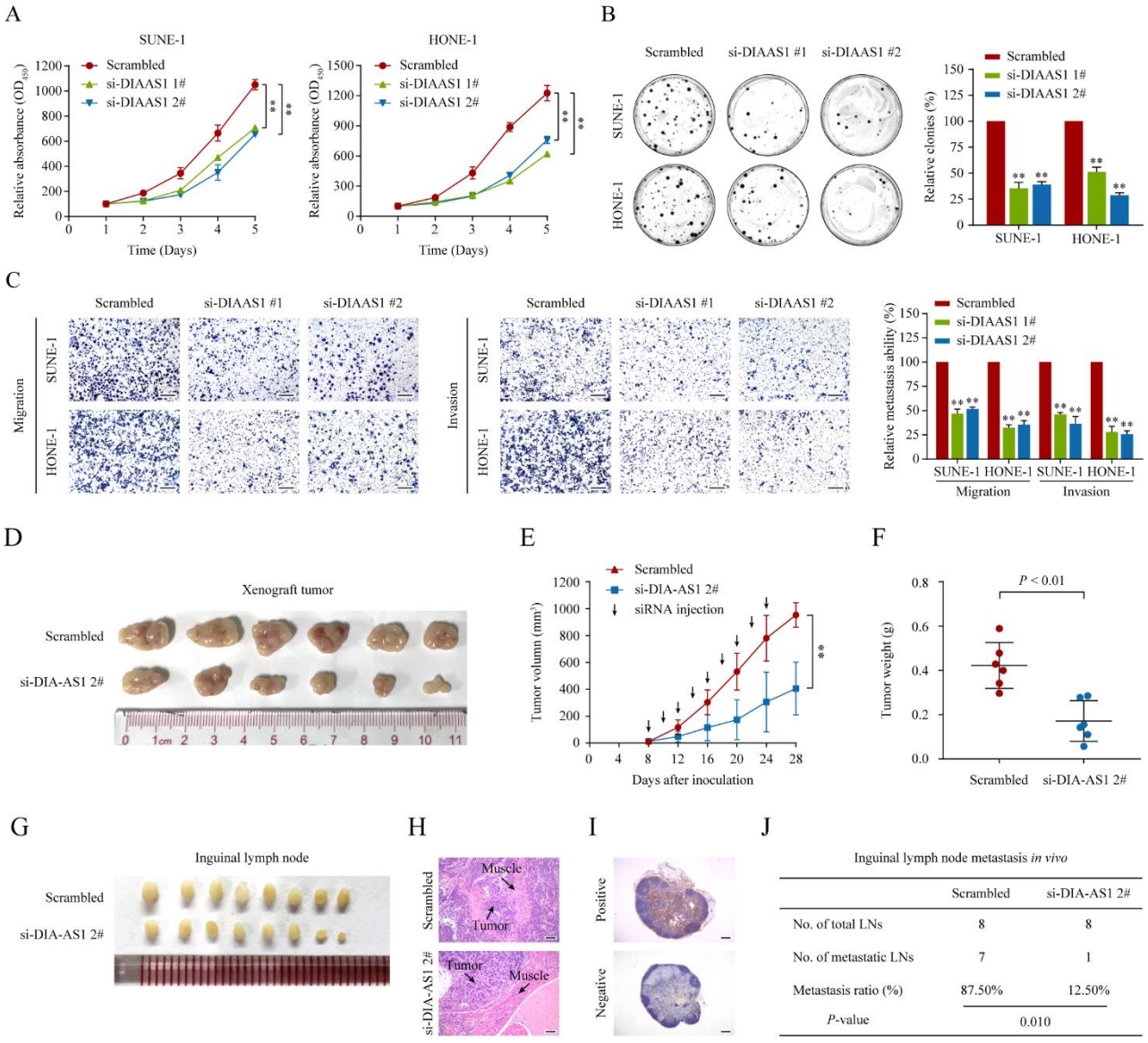

Supplemental Figure S5. *DIAPH1-AS1* interference suppresses NPC proliferation and metastasis *in vitro* and *in vivo*.

A–C. SUNE-1 and HONE-1 cells were transfected with siRNAs targeting *DIAPHA1-AS1* or the corresponding negative control. CCK-8 proliferation (**A**), colony formation (**B**), and Transwell migration/invasion assays (**C**) were conducted to assess cell proliferation, migration, and invasion, respectively. Scale bar: 200 μm. **D–J.** SUNE-1 cells were subcutaneously injected into the nude mice (n = 6) to build a xenograft tumor model (**D–F**) and into the footpads of nude mice (n = 8) to build an inguinal lymph node metastasis model (**G–J**). After one week of growing, the cholesterol-conjugated siRNA 2# targeting *DIAPH1-AS1* or the scrambled siRNA was injected locally into the tumors once every two days (3nmol per tumor), for nine times totally. (**D**) The representative image of xenograft tumors resected from nude mice. (**E**)

The tumor growth curves determined by measuring the tumor volumes. (**F**) The weight of xenograft tumors harvested from nude mice. (**G**) The representative image of inguinal lymph nodes resected from nude mice. (**H**) The representative microscopy images showing the H&E staining of footpad tumors. Scale bar: 100μm. (**I**) The representative images of inguinal lymph nodes with positive (top panel) and negative (bottom panel) pan-cytokeratin staining. Scale bar: 250μm. (**J**) The pan-cytokeratin staining results of inguinal lymph nodes in mice of each group. Data are presented as the mean ± SD. $*P < 0.05$, $**P < 0.01$.

Supplementary Figure S6

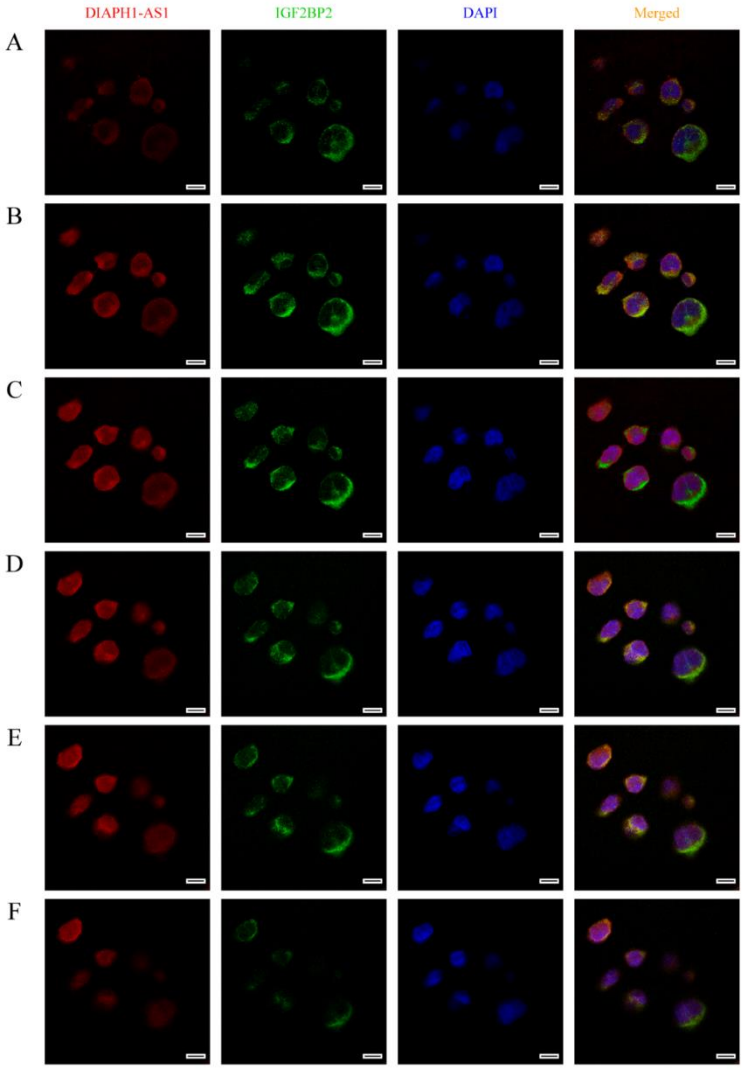

Supplemental Figure S6. Z-Stack of HONE-1 cells reflecting the co-localization of *DIAPH1-AS1* and IGF2BP2 in the cytoplasm.

A–F. Z-Stack was performed using a laser confocal microscope (Zeiss LSM-880 Fast AiryScan, Germany). An image of the cell was taken on several planes, ranging from upper to lower layers. *DIAPH1-AS1* was staining red (Cy3), IGF2BP2 was staining green (fluorescent secondary antibodies), and the nuclei were stained blue (DAPI). (**A**) Upper image of cells. (**B–F**) Every next image was taken in one μm deeper than the previous one.

Supplementary Figure S7

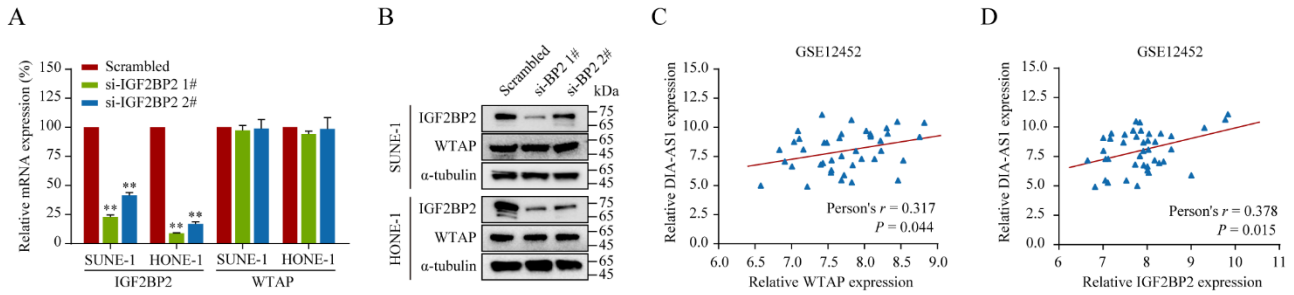

Supplemental Figure S7. WTAP-mediated m^{6}A modification of lncRNA *DIAPH1-AS1* maintains its IGF2BP2-dependent stability.

A–B. Quantitative RT-PCR (**A**) and western blotting (**B**) analysis of IGF2BP2 and WTAP expressions in SUNE-1 and HONE-1 cells with or without IGF2BP2 silencing. GAPDH or α-tubulin served as internal controls. **C–D.** Correlation analysis between WTAP and *DIAPH1-AS1* expression (**C**), and between IGF2BP2 and *DIAPH1-AS1* expression (**D**) based on the GEO database (GSE12452). Data are presented as the mean ± SD. **P* < 0.05, ***P* < 0.01. The experiments were repeated independently at least three times.

Supplementary Figure S8

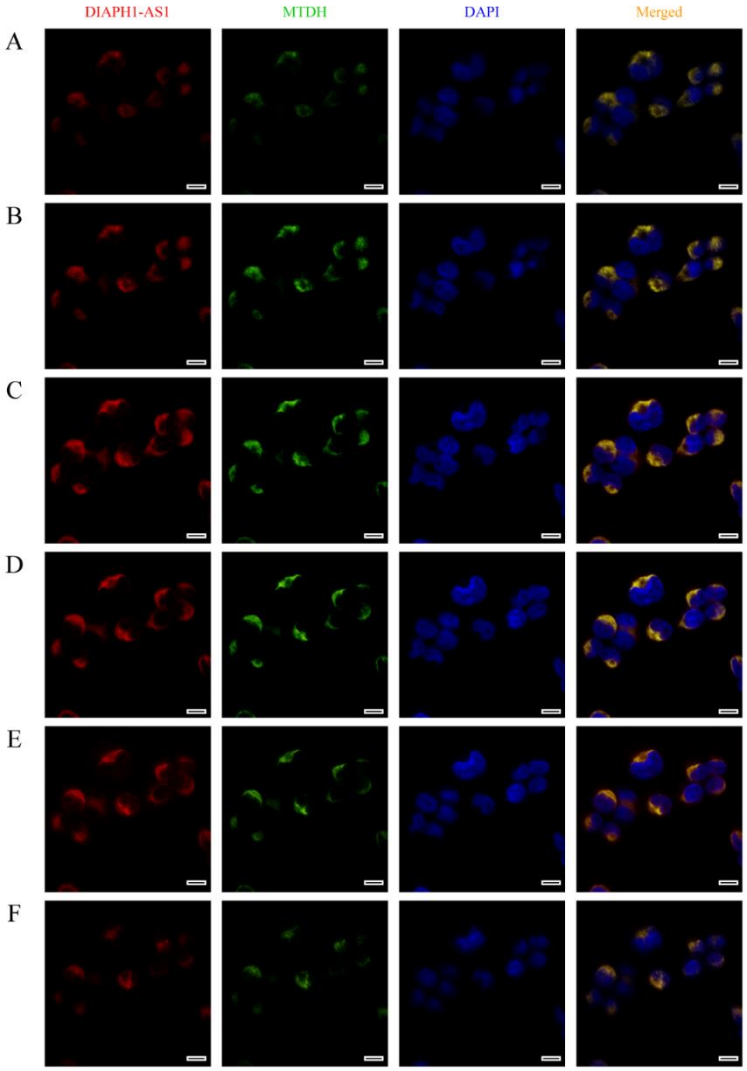

Supplemental Figure S8. Z-Stack of HONE-1 cells reflecting the co-localization of *DIAPH1-AS1* and MTDH in the cytoplasm. Z-Stack was performed as in Supplementary Figure S6, but stained MTDH protein with green (fluorescent secondary antibodies).

Supplementary Figure S9

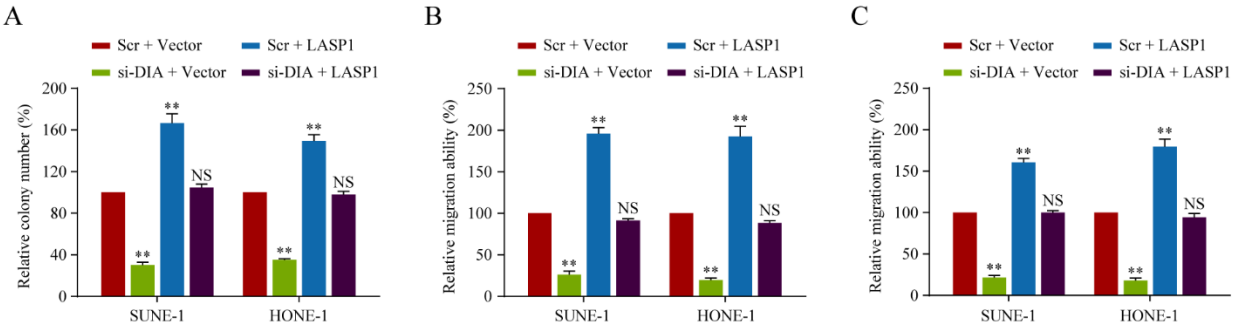

Supplemental Figure S9. LASP1 is the prime functional target of *DIAPH1-AS1*-mediated proliferation and metastasis in NPC.

A. The statistical analysis results of colony formation assays in NPC cells co-transfected with si-*DIAPH1-AS1* and LASP1 overexpressing vectors or the corresponding negative control (**Figure 7 G**). **B–C.** The statistical analysis results of Transwell migration and invasion assays in NPC cells co-transfected with si-*DIAPH1-AS1* and LASP1 overexpressing vectors or the corresponding negative control (**Figure 7 H–I**). Data are presented as the mean ± SD. **P* < 0.05, ***P* < 0.01, NS = no significance. The experiments were repeated at least three times independently.